centered at 95 GHz. The bandwidth may be increased, if necessary, by adding probes to the hybrid [6], or by substituting another type of E-plane hybrid [11]. The housing utilized in this demonstration model can be greatly simplified by eliminating three of the four waveguide bends. (Two bends were used only in characterizing the hybrid, and a third bend could be replaced by a straight housing section.)

The E-plane approach provides advantages in terms of printed-circuit economy, effective shielding, high unloaded $Q(>400$ at 94 GHz), low equivalent dielectric constant (for eased production tolerances), and simple transitions to standard waveguide. The E-plane mixer is applicable to a wide range of advanced millimeter-wave systems including radars, communication links, and radiometers.

ACKNOWLEDGMENT

The work reported was sponsored by Eaton Corporations AIL Division, under the direction of M. Lebenbaum, B. Peyton, and J. Whelehan. The diodes were developed by J. Calviello and P. Bie of AIL's Central Research Laboratory under the direction of J. Taub. Technical assistance was provided by A. Cooley, A. Kunze, J. Pieper, A. Rees, and C. Thompson all of the AIL Division.

REFERENCES

[1] T H Oxley *et al*, "Hybrid microwave integrated circuits for millimeter wavelengths," in *Dig 1972 MTT Symp.*, May 1972, pp 224–226.
[2] T Araki and M Hirayama, "A 20-GHz integrated balanced mixer," *IEEE Trans Microwave Theory Tech*, vol. MTT-19, pp 638–643, July 1971.
[3] A K. Gorwara *et al*, "*K*-band image-reject and *Ka*-band balanced mixers constructed using planar millimeter-wave techniques," SRI Final Rep, Contract N00123-74-C-1957, Mar. 1975
[4] P J Meier, "Printed-circuit balanced mixer for the 4- and 5-mm bands," in *Dig. 1979 MTT Symp.*, Apr. 1979, pp. 84–86
[5] P J Meier, "Millimeter integrated circuits suspended in the E-plane of rectangular waveguide," *IEEE Trans Microwave Theory Tech.*, vol MTT-26, pp 726–773, Oct 1978.
[6] P. J. Meier, "Printed-probe hybrid coupler for the 3-mm band," in *Proc. 9th Eur Microwave Conf*, Sept 1979, pp 443–447
[7] P. J. Meier, "E-plane components for a 94-GHz printed-circuit balanced mixer," in *Dig 1980 MTT Symp.*, May 1980, pp. 267–269.
[8] P. H Vartanian *et al*, "Propagation in dielectric slab-loaded rectangular waveguide," *IRE Trans. Microwave Theory Tech.*, vol MTT-6, pp 215–222, Apr 1958
[9] J. A. Calviello, J. L Wallace, and P. R Bie, "High-performance GaAs beam-lead mixer diodes for millimeter and submillimeter applications," *Electron Lett*, vol 15, no 17, pp. 509–510, Aug 1979
[10] J A Calviello, S. Nussbaum, and P R Bie, "High-performance GaAs beam-lead mixer diodes for millimeter and submillimeter applications," in *Dig IEEE Int Electron Devices Meeting*, Dec 1981, pp 692–695
[11] E Kpodzo, K Schunemann, and G. Begemann, "A quadriphase fin-line modulator," *IEEE Trans. Microwave Theory Tech.*, vol. MTT-28, pp. 747–752, July 1980.

A Cryogenic Millimeter-Wave Schottky-Diode Mixer

ERIK L. KOLLBERG, MEMBER, IEEE,
AND HERBERT H. G. ZIRATH

***Abstract*—We report theoretical calculations and measurements on cryogenic millimeter-wave Schottky-diode mixers. Measurements of the embedding impedances at the signal and image frequencies have been used for the theoretical predictions of the mixer performance, and an excellent agreement with measured performance was obtained. Measurements of embedding impedances for various waveguide structures are reported, and the choice of configuration for optimum single-sideband performance is discussed.**

Manuscript received May 5, 1982; revised July 28, 1982. This work was supported (in part) by the Swedish Board for Technical Development

The authors are with the Department of Electron Physics I and Onsala Space Observatory, Chalmers University of Technology, Göteborg, Sweden

I. INTRODUCTION

Cooled millimeter-wave Schottky-diode mixers are frequently used in low-noise radiometer systems [1]–[4]. Although the superconducting semiconductor–insulator–semiconductor (SIS) mixer has still lower noise [5], it needs cooling to 4.2 K or below, while there is no use cooling the diode mixer below about 20 K [6]. Therefore, for most practical purposes, cooled diode mixers are at present the best choice for low-noise receivers. Below, we will report on some results obtained when developing the mixer receivers now in use at Onsala Space Observatory.

II. MIXER DESIGN

The mixers used are designed in a straightforward way (Fig. 1). An impedance transformer at the IF-output port matches the 50-Ω IF amplifier to the diode when dc-biased to have a differential dc-resistance $r = (di/dv)^{-1}$ equal to 175 Ω. This impedance level has been found to be a good compromise yielding a low-power reflection (less than about 1–2 dB extra conversion loss) for most bias conditions and the backshort settings where low-noise operations are obtained. The diode is mounted in a reduced-height waveguide in order to facilitate impedance matching. In Fig. 2, a typical locus of the diode impedance (the complex conjugate) versus dc- and local-oscillator bias is shown. The waveguide cross-section dimensions, the length and the shape of the whisker, the low-pass filter impedance, and the position of the diode chip in the waveguide are the most important parameters that influence the locus of the impedance circle, representing the embedding impedance seen by the diode, obtained when the backshort (l_b) is moved over $\lambda_g/2$ (see Fig. 2).

In Fig. 3, an equivalent embedding circuit is shown. The inductive (X_L) and capacitive (X_{C1}, X_{C2}) circuit elements, however, cannot be represented by simple inductances and capacitances [7]. For the fundamental frequency band of the waveguide (no higher modes can propagate), the embedding impedance can be measured as described in [8] and [9]. In Figs. 4 and 5, measurements on some experimental mixers made using the method described in [8] are depicted. From these measurements, X_L, X_{C1}, and X_{C2} of Fig. 3 can be determined.

It is interesting to see how shortening the whisker not only moves the impedance circle downwards in the impedance diagram (corresponding to smaller inductance X_0 and X_L), but also makes the diameter of the impedance circle smaller (corresponding to a decrease in X_{C1}). In Fig. 5, the effect of going from an ordinary reduced-height waveguide to a ridged waveguide by making grooves is illustrated (Fig. 5(a) and (b)). The decrease in the waveguide impedance is observed as a decrease in the impedance circle diameter. By further decreasing the whisker length, the position of the circle moves, corresponding to a lower inductance X_L.

Short enough whisker wires (Figs. 4 and 5(c)) will leave impedance circles with diameters close to the impedance of the waveguide, indicating that X_{C1} is large compared to X_L. Similar observations have been made by Pospieszalski and Weinreb [9], [10].

0018-9480/83/0200-0230$01.00 ©1983 IEEE

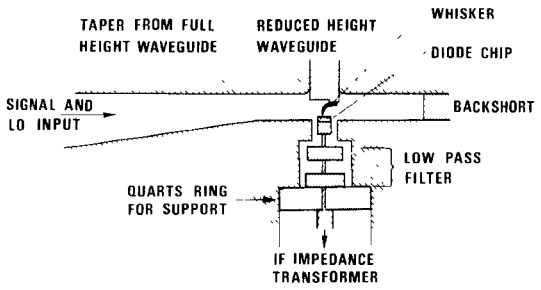

Fig. 1. Schematic diagram of the waveguide mixer mount.

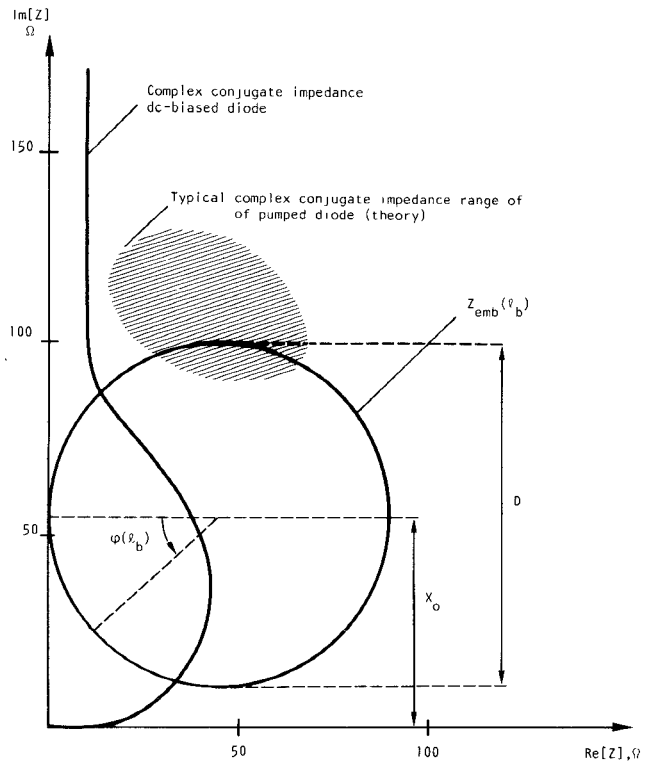

Fig. 2. The locus of the embedding impedance as seen from the diode versus backshort setting, and the locus of the complex conjugate impedance of the dc-biased diode at 100 GHz, with $\phi = 1080$ mV, $C_0 = 14.5$ fF, $kT/q = 28.5$ mV, $i_0 = 4.9 \cdot 10^{-14}$ mA, and $R_s = 10\ \Omega$. $\varphi(l_b)$ is increasing when the backshort is moved towards the diode mount. The shaded area indicates the approximate impedance of the pumped diode.

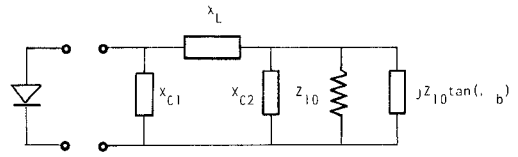

Fig. 3. The equivalent circuit of the embedding impedance for fundamental waveguide mode frequency range. The inductive reactance X_L is related to the whisker inductance. X_{C1}/X_L is important for the diameter and location of the impedance circle (Fig 2) (see [8]). For very reduced height waveguide mount X_{C1} and X_{C2} can, to a first approximation, be assumed large.

III. Theoretical Evaluation

In order to evaluate a mixer properly, one has to know the diode impedance and noise properties, and the embedding circuit impedances at all harmonics of the local oscillator frequency f_{LO}, as well as at all harmonic sidebands ($nf_{LO} \pm f_{IF}$). In the theory by Held and Kerr, the diode is modeled in the usual way, i.e., an ideal exponential diode is in parallel with a variable capacitance and in series with a current independent series resistance. The

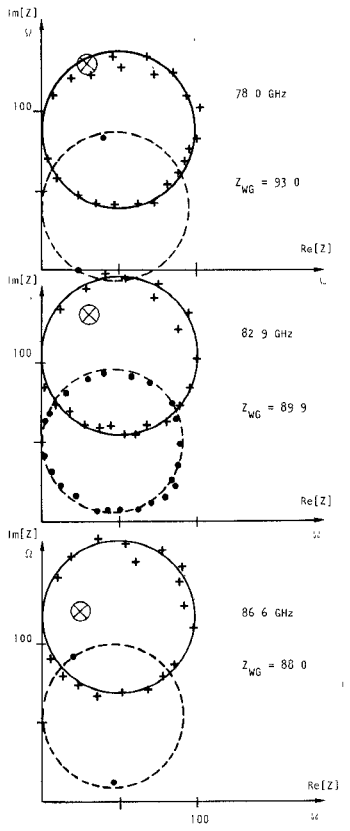

Fig 4 Impedance loci for the 70–95-GHz mixer. The full line circles are for the longest whisker, while the broken line circles are for the shortest whisker.

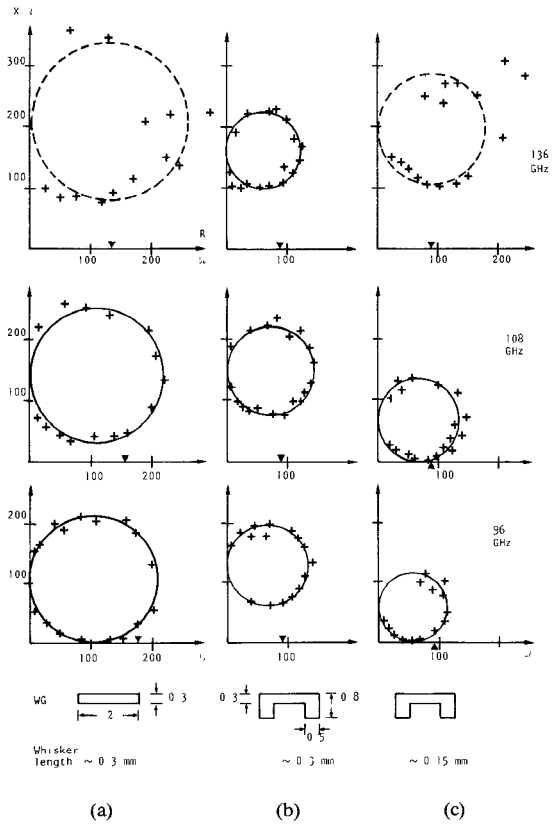

Fig. 5. Impedance loci for a successively modified 90–140-GHz mixer mount. Each column is for one mount and three different frequencies (96, 108, and 137 GHz). The cross section and approximate whisker length are given below each column

diode is assumed to give shot noise, and the series resistance pure thermal noise. In the theory, the properties of the embedding network are also accounted for. However, modeling the diode at high forward currents is not straightforward since the exponential voltage dependance of the current is not constant due to microcluster effects at the metal–semiconductor interface [13], and a current dependent excess noise is generated [11]–[13]. Examples are given in Figs. 6 and 7.

The embedding impedances at the signal and the image frequency are the most important ones, and have been measured for the mixers described in this paper. However, the harmonic sideband impedances cannot be determined for the actual mounts unless a scaling experiment, as described by Held and Kerr [11], is used. In the computer runs below, we have estimated the harmonic impedances, assuming X_L to scale approximately linearly with frequency, and X_{C1}, X_{C2}, and $\tan(\beta l) Z_{wg} \approx \infty$. This is to some extent justified by the results by Held and Kerr [11], and by the fact that a reasonable agreement is obtained between theory and experiments. It was also found that in order to describe theoretically the main features of the measured properties, taking into account two harmonics is usually sufficient.

The Pt–GaAs diodes used in the experiments described here were made from molecular beam epitaxy GaAs and supplied by Dr. A. Y. Cho and Dr. M. Schneider at the Bell Telephone Laboratories, Crawford Hill, NJ. The diode properties necessary for the theoretical evaluation were investigated [13], and a shot-noise temperature of $nT_0/2 = 40$ K at low currents (Fig. 6) and a zero bias capacitance of 14.5 fF was found. The Mott character of the diode capacitance versus bias-voltage was accounted for, although using an ordinary Schottky-diode capacitance $C_0 \cdot (1 - v/\phi)^{-0.45}$ or the Mott character of the diode did not give a considerably different result, as long as the capacitance versus voltage was correct for large forward bias (where it has the Schottky character anyway). The potential ϕ was assumed equal to 1080 mV at 20 K [13].

Since the I–V characteristic has a somewhat peculiar shape (Fig. 6), one has to be careful when defining the series resistance R_s from the equation

$$i = i_0 \left[\exp\left(\frac{v - iR_s}{v_0} \right) - 1 \right] \tag{1}$$

where $v_0 = \eta T \cdot k/e$. We have obtained R_s as shown in Fig. 6, and used the experimental I–V characteristic in the computations. The dc series resistance is typically 8–10 Ω, which increases to 12–15 Ω at 100 GHz due to the skin effect. The noise temperature increase at high forward currents (Fig. 7) has been suggested to be caused by hot electron noise in the epilayer of the diode [11], [12]. Due to the difficulties in properly taking this extra noise contribution into account theoretically, we have omitted this in the calculations reported below. It should be pointed out that the computer calculations show that 20-K thermal noise from the series resistance contributes to the mixer noise with between 10 and 20 K typically (see Fig. 12), and that the computed mixer noise is normally a few tens of degrees lower than the measured mixer noise.

IV. Measurements of Conversion Loss and Noise

The IF amplifier of the cooled (18-K) mixer receiver is a 3.7–4.2-GHz (18-K) parametric amplifier followed by a cooled (60-K) FET amplifier. The overall IF-noise temperature at the diode is 24 K. An impedance transformer between the low-pass filter and the 50-Ω input port of the parametric amplifier makes the diode see 175 Ω at 4 GHz. The noise temperature of the

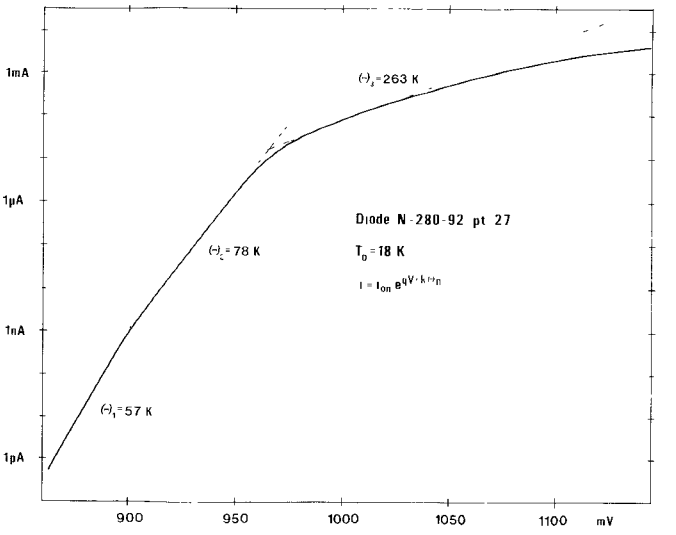

Fig. 6. Typical $\log(I)$–V characteristic at 20 K for the N280–92 diode.

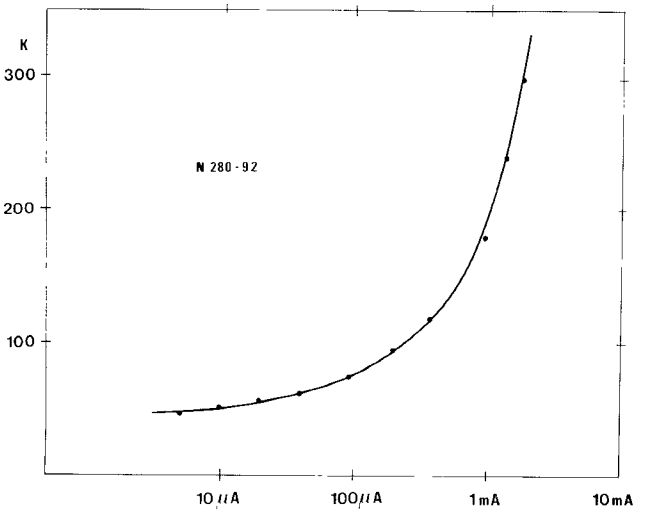

Fig. 7. Typical effective diode noise temperature versus current measured at 4 GHz for the dc-biased N280–92 diode at 20 K.

system was measured using a room-temperature and a liquid nitrogen cooled load in front of the window of the receiver dewar. The noise temperature was measured over the 3.7–4.2-GHz IF band using a narrow-band (1-MHz) precision receiver.

The noise temperature versus IF frequency was found to vary typically with about 20 percent. In the experiments discussed below, we quote a mean over the IF band.

The single-sideband response was measured using another mixer mount used to multiply the output of a 8–12-GHz sweeper to the actual frequency range. We found that the (noncontacting) backshort could suppress one sideband better than −20 dB. The single-sideband noise temperature versus backshort position was measured as follows.

a) Set the backshort to cancel one sideband (e.g., the lower sideband) and measure the noise temperature of the system, which is then considered to be the single-sideband noise temperature $T_{SSB,0}$ (upper sideband).

b) Inject the coherent signal and measure the ratio of the coherent signal power to the noise power. Hence, the coherent signal power is *calibrated in degrees Kelvin*.

In this way, a "narrow-band noise source" is obtained which

may be used for evaluating the single-sideband system noise temperature. In order to evaluate the conversion loss, we must know the IF-amplifier noise (T_{IF}), which consists not only of the noise from the IF-amplifier itself, but also from noise from the IF-amplifier input circulator (T_0), which is reflected back from the mixer ($|\Gamma_{mix}|^2 \cdot T_0$). More details of the full measuring procedure will be published elsewhere.

V. Measurements on the 60–90-GHz Mixer

The system noise temperature of a single-sideband mixer receiver can be written as

$$T_{syst} = T_A\left(1 + \frac{L_s}{L_t} + L_s \cdot \sum_{n=2}^{\infty}\left(\frac{1}{L_{n+}} + \frac{1}{L_{n-}}\right)\right) + T_{MXR} + L_s \cdot T_{IF} \tag{2}$$

where T_A is the antenna temperature, here assumed to be the same at the image frequency with conversion loss L_t and at the upper and lower harmonic sidebands, with conversion loss L_{n+} and L_{n-}, respectively. L_s is the signal conversion loss, T_{MXR} the inherent single-sideband noise of the mixer itself, and T_{IF} the noise temperature of the intermediate frequency amplifier. From (2), it can be seen that in practical applications it may be advantageous to have L_t and $L_{n\pm}$ large compared to L_s. A large L_t can be obtained using the backshort positioned so that the image frequency is short-circuited at the diode, i.e., $l_{bs} = n \cdot \lambda_{gi}/2$. However, this puts a constraint on T_{MXR} and L_s that can then be minimized only by the dc bias, the amount of applied LO power, and by changing l_{bs} in steps of $\lambda_{gi}/2$.

We found that, for the 70–100-GHz mixer, it was advantageous to operate the mixer over the frequency range 75–95 GHz having the backshort short-circuiting the lower sideband. Fig. 8 depicts the receiver noise temperature $T_{rec} = T_{MXR} + L_s \cdot T_{IF}$ versus frequency for this mode of operation, and for three different lengths of the whisker. The embedding impedance versus backshort position of the longest whisker and the shortest one is shown in Fig. 4.

The position of the backshort for the data shown in Fig. 8 was one wavelength at the lower sideband frequency away from the diode, i.e., the lower sideband was short-circuited.

The theoretical curves of Fig. 8 were obtained assuming the harmonic impedances equal for the three cases and using the nonlinear analysis made for 85 GHz for the whole frequency range. The result clearly demonstrates two effects. First, increasing the length of the whisker, i.e., in the first approximation increasing the whisker inductance, tunes the mixer to lower frequencies. It is also seen that, at least for this particular mode (short-circuited lower sideband), the shortest whisker yields the better performance over the examined frequency range (the corrugated feed horn used was cut off at 70 GHz).

Fig. 9 shows the system noise temperature for the system as used in the 20-m dish at the Onsala Space Observatory. The short whisker is used, but the backshort position is chosen for lowest system noise, i.e., either $\lambda_{gi}/2$, λ_{gi}, or $3\lambda_{gi}/2$. The full lines demonstrate the theoretical results, which are in very good agreement with the measured performance.

VI. Measurements on the 90–140-GHz Mixer

The advantages were less pronounced operating this mixer with a short-circuited image frequency. The diodes used had a capacitance a factor of 1.3 lower than that for the 70–95-GHz mixer,

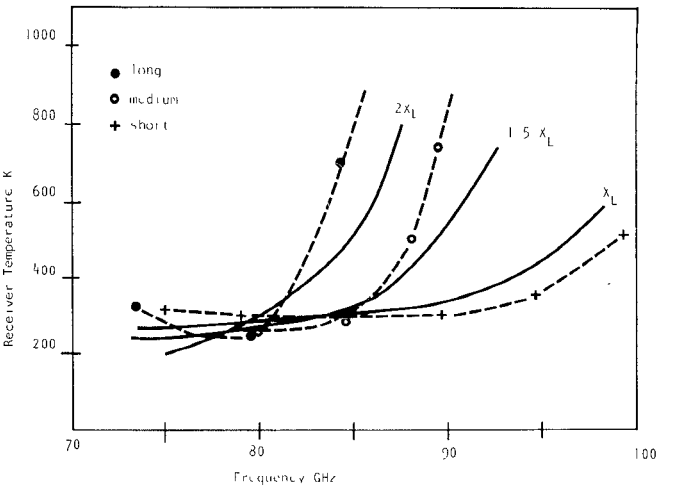

Fig. 8. Receiver noise temperature versus frequency for the 70–95-GHz mixer for three different lengths of the whisker. X_L and $2X_L$ correspond to the short and long whisker, respectively, discussed in Fig. 4. The broken line indicates the experimental result, and the full line the theoretical result. Only the two first harmonic impedances were considered.

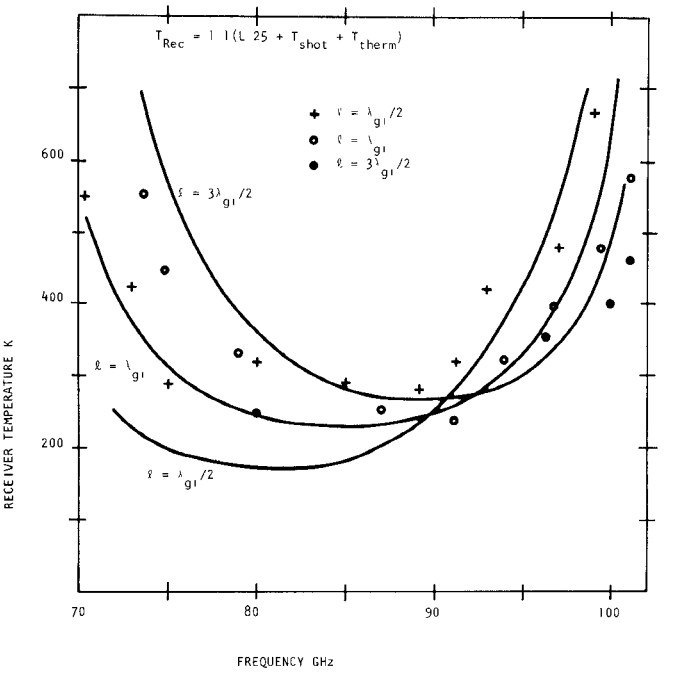

Fig. 9. Receiver noise temperature of the 70–95-GHz Onsala system. The whisker is "short" and the full lines indicate the theoretically derived noise temperature $T_{Rec} = 1.1(L_s \cdot 24 + T_{shot} + T_{therm})$. Only the two first harmonic and harmonic sidebands are accounted for theoretically.

which should roughly compensate for the higher frequency. The waveguide height (0.2 mm) and the waveguide width (2.0 mm) were decreased with a factor 1.5, and the whisker was made very short. The resulting embedding impedance circles then very much corresponded to those for the short whisker in Fig. 4.

The input reactance of the low-pass filter at the signal frequency will affect the embedding impedance, and should, in the first place, affect the "whisker inductance" reactance X_L. We changed the filter in order to increase the theoretical capacitive reactance of the filter from $-j10\ \Omega$ to $-j30\ \Omega$ at 106 GHz. A decrease in X_L of $15 \pm 5\ \Omega$ was then measured, and a somewhat better performance at higher frequencies was observed.

Although several design parameters of the 60–90-GHz mixer

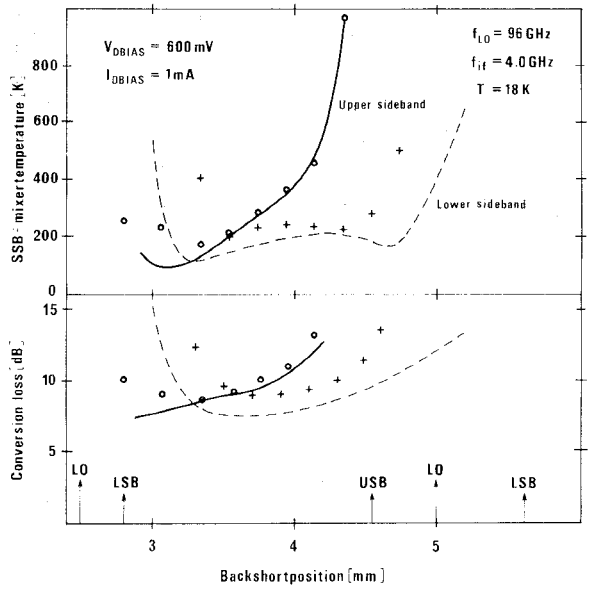

Fig. 10. An example on noise temperature and conversion loss for the 90–140-GHz mixer cooled to 20 K. The theoretical conversion loss has been adjusted 2 dB to account for circuit losses.

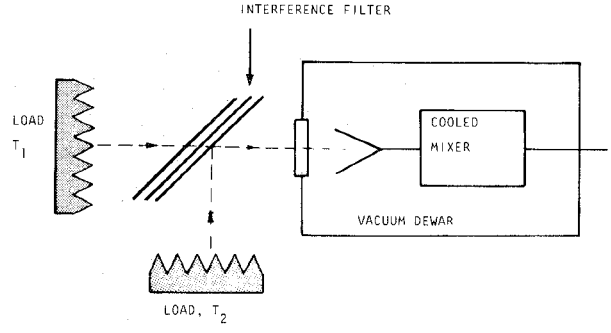

Fig. 11. Experimental setup for investigation of harmonic sideband response (at 200 GHz).

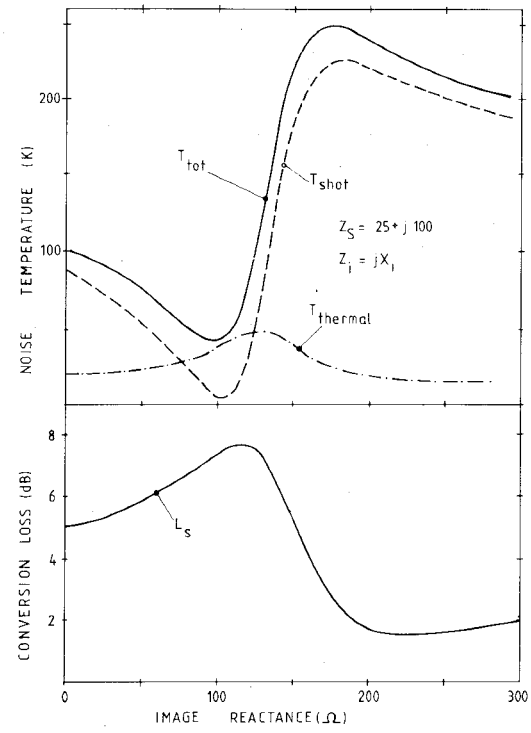

Fig. 12. Theoretical mixer noise and conversion loss for an 80-GHz diode mixer cooled to 20 K versus image reactance. The diode zero bias capacitance is 10.6 fF and series resistance 15 Ω. The signal input impedance $25 + j100$ Ω. The harmonic frequency impedances are assumed equal to $50 + j250$ Ω.

could be scaled to the 90–140-GHz frequency band (waveguide dimensions, whisker length) it was necessary, in this case, to stay with the 4-GHz IF frequency, and to introduce the smooth step in the waveguide (Fig. 1) in order to have a larger waveguide height of the backshort section, which facilitated the manufacturing of the noncontacting short. This step causes the backshort reactance in the diode plane not to vary like $jZ_0 \tan(\beta l)$, as in the 75–95-GHz mixer where no step was necessary.

Fig. 10 shows conversion-loss and mixer noise temperature versus back-short position at 96 GHz obtained experimentally as well as theoretically. There is a discrepancy for the conversion loss between theory and experiments which can be explained by losses in the experimental setup. For similar experiments at 110 GHz and 140 GHz, the agreement between theory and experiment was also good.

One experiment was also made to evaluate the harmonic response, i.e., the ratio

$$L_s \cdot \sum_{n=2} \left(\frac{1}{L_{n+}} + \frac{1}{L_{n-}} \right)$$

appearing in (1). The experimental technique is shown in Fig. 11. A quasioptical interference filter is frequency selective, i.e., the signal at 200 GHz is propagating straight through the filter while 100 GHz is reflected almost entirely. Measuring the system noise temperatures from the two different positions A and B using a room-temperature absorber and a liquid nitrogen cooled absorber suggested that

$$L_s \cdot \sum_{n=2}^{\infty} \left(\frac{1}{L_{n+}} + \frac{1}{L_{n-}} \right) \simeq 0.08 \text{ at } 96 \text{ GHz}.$$

VII. Optimizing the Mixer Performance

From the results reported above, we can draw the conclusion that knowing the signal and image impedances is far more important than knowing the harmonic and harmonic sideband impedances. The agreement demonstrated between theory and the experimental results also gives us some confidence in using the theory for optimizing the circuit. Again, an interesting case exists when the image frequency is reactively loaded, i.e., when the backshort short-circuits the diode mount (compare Figs. 3 and 4). Fig. 12 shows how the mixer noise temperature and the conversion loss ($T_{IF} = 0$) varies versus the image reactance. The impedances at the signal frequency are chosen to $25 + j100$, which is close to optimum, while at the harmonics and harmonic sidebands the impedances are assumed to be highly inductive, viz., $Z_2 = 50 + j200$, $Z_n = 50 + j250$, $n = 3$ to 6. It is interesting to notice the minimum in the mixer noise near $jX_i = j100$ Ω where the shot noise is as low as 4 K. Actually, for X_i larger than 100 Ω, parametric effects due to the pumped capacitance become important, which is why this region should be avoided (notice the low-conversion loss for $X_i = 200$ Ω, which is due to parametric effects). The result suggests that an image reactance equal to or smaller than the signal reactance is essential. This case can be achieved if the whisker inductance is low enough and for the lower sideband short-circuited (compare Fig. 2). It is interesting to point out that this is exactly the case for the 70–95-GHz mixer.

A more detailed discussion concerning the optimization procedure will be presented in a forthcoming report.

ACKNOWLEDGMENT

The authors would like to acknowledge Dr. A. Kerr at the Goddard Space Institute, NY, for kindly lending us his computer program, and T. Ståhlberg for some calculations on mixer performance. They would also like to thank C. O. Lindström for carrying through many of the experiments.

REFERENCES

[1] R. A Linke, M. V. Schneider, and A. Y. Cho, "Cryogenic millimeter-wave receiver using molecular beam epitaxy diodes," *IEEE Trans. Microwave Theory Tech.*, vol. MTT-26, pp. 935–938, 1978.
[2] N. Keen, R. Haas, and E. Perchtold, "Very low noise mixer at 115 GHz using a Mott diode cooled to 20 K," *Electron. Lett*, vol. 14, pp. 825–826.
[3] A. V. Räisänen, N. R. Erickson, J. L. R. Marrero, P. F. Goldsmith, and C. R. Predmore, "An ultra low-noise Schottky mixer receiver at 80–120 GHz," presented at the 1981 IEEE Int. Conf. on Infrared and Millimeter Waves, Miami Beach, Florida, Dec. 7–12, 1981.
[4] B. Vowinkel, J. K. Peltonen, W. Reinhert, K. Grüner, and B. Aumiller, "Airborne imaging system using a cryogenic 90-GHz receiver," *IEEE Trans. Microwave Theory Tech.*, vol. MTT-29, pp. 535–541, 1981.
[5] M. Feldman and S. Rudner, *Reviews Infrared Millimeter Waves*, vol. II, 1982.
[6] T. J. Viola and R. J. Mattauch, "Unified theory of high-frequency noise in Schottky barriers," *J Appl. Phys.* vol 44, pp. 2805–2808, 1973.
[7] R. L. Eisenhart and P. J. Kahn, "Theoretical and experimental analysis of a waveguide mounting structure," *IEEE Trans. Microwave Theory Tech.*, vol. MTT-19, pp. 706–719, 1971.
[8] C. E. Hagström and E. L. Kollberg, "Measurements of embedding impedance of millimeter-wave diode mounts," *IEEE Trans. Microwave Theory Tech.*, vol. MTT-28, pp. 899–904, 1980.
[9] M. Pospieszalski and S. Weinreb, "A method for measuring an equivalent circuit for waveguide-mounted diodes," in *Proc. 10th Eur. Microwave Conf.* (Warszawa, Poland), Sept. 1980.
[10] M. Pospieszalski and S. Weinreb, "A method for measuring an equivalent circuit for waveguide-mounted diodes," National Radio Astronomy Observatory, Charlottesville, VA, Electronics Division Internal Rep. 201, Oct. 1979.
[11] N. H. Held and A. R. Kerr, "Conversion loss and noise of microwave and millimeter-wave mixers: Parts 1 and 2," *IEEE Trans. Microwave Theory Tech.*, vol. MTT-26, pp. 55–70, Feb. 1978.
[12] N. J. Keen, "Low-noise millimeter-wave mixer diodes, results and evaluation of a test programme," *Proc IEEE*, vol. 127, pp. 188–198, Aug. 1980.
[13] H. Zirath, E. Kollberg, M. V. Schneider, A. Y. Cho, and A. Jelenski, "Characteristics of metal-semi-conductor junctions for mm-wave detectors," in *Proc. 7th Int. Cont. Infrared millimeter waves*, (Marseille, France), Feb. 1983.

Hyperabrupt Junction Varactor Diodes for Millimeter-Wavelength Harmonic Generators

KEITH LUNDIEN, MEMBER, IEEE,
ROBERT J. MATTAUCH, SENIOR MEMBER, IEEE, JOHN ARCHER,
AND ROGER MALIK, MEMBER, IEEE

***Abstract*—The design of a hyperabrupt Schottky-barrier varactor is considered with an exponentially retrograded doping profile assumed. Resistance and capacitance models are used to determine optimum doping profile characteristic length and breakdown voltage with respect to device dynamic cutoff frequency. Device fabrication is discussed and test results are presented indicating conversion efficiencies of approximately 15 percent upon doubling to the 200-GHz frequency range.**

Manuscript received June 2, 1982; revised September 9, 1982. This work was supported in part by the National Science Foundation under Grant EC580-22937, and by the National Radio Astronomy Observatory which is operated by Associated Universities, Inc., under contract with the National Science Foundation.

K. Lundien is presently with General Electric, Portsmouth, VA.
R. Mattauch is with the Department of Electrical Engineering, University of Virginia, Charlottesville, VA.
J. Archer is with the National Radio Astronomy Observatory, Charlottesville, VA.
R. Malik is with the U.S. Army Electronics Technology and Devices Laboratory, ERADCOM, Fort Monmouth, NJ 07703.

I. INTRODUCTION

Due to recent improvements in the conversion efficiency, and output power of GaAs-Schottky-barrier varactor harmonic generators, solid-state sources are replacing expensive and short-lived klystrons as local oscillators in the 100–230-GHz range. This paper extends the work of Archer *et al.* [1] in the optimization of devices for harmonic generation by taking advantage of the increased voltage sensitivity of hyperabrupt junction device capacitance.

For the same voltage variation, the capacitance of a hyperabrupt junction changes more than that of a comparable abrupt junction device. This results in a greater power conversion efficiency because the relative magnitude of each output harmonic depends upon the nonlinearity of the capacitance–voltage law. This paper is concerned with the selection of the optimal device fabrication parameters: impurity doping profile, epitaxial layer thickness, and anode size to provide the maximum cutoff frequency and output power for a given breakdown voltage.

II. DEVICE STRUCTURE

The impurity doping profile examined in this study was exponentially retrograded as shown in Fig. 1. The doping in the epitaxial layer is given by

$$N_D(x) = N_0 \exp(-x/L)$$

where N_0 is the impurity atom concentration at the surface, and L is the characteristic length of the exponential decay. Application of Poisson's equation, and the depletion region approximation, yields the voltage across the depletion region width W as

$$V(W) = -\frac{q}{\epsilon} N_0 L^2 \left[\left(\frac{W}{L} + 1 \right) e^{-W/L} - 1 \right]. \quad (1)$$

The reverse breakdown voltage V_{br} for a particular combination of N_0 and L was found by determining the depletion region width $H = W(V_{\text{BR}})$ at the onset of avalanche breakdown by setting the ionization integral equation to unity

$$1 = \int_0^H A \exp\left[-\frac{b^2}{E^2(x)} \right] dx \quad (2)$$

where $A = 3.5 \times 10^5$ cm^{-1} and $b = 6.85 \times 10^5$ V cm^{-1} for GaAs as given by Sze and Gibbons [2].

The thickness of the undepleted epitaxial layer was set equal to the maximum depletion region width H, determined above in order to minimize its contribution to the device series resistance.

III. EQUIVALENT CIRCUIT

The varactor diode can be modeled as a junction capacitance in series with the resistance of the epitaxial layer and the substrate. Including the edge effects of a small anode radius, the junction capacitance is given by [3]

$$C = \frac{\epsilon_0 \epsilon_r \pi r^2}{W} \left(1 + \frac{\gamma W}{r} \right) \quad (3)$$

where r is the anode radius, ϵ_0 is the permittivity of free space, ϵ_r

0018-9480/83/0200-0235$01.00 ©1983 IEEE